

Highlights

Chart Specification: Structural Representations for Incentivizing VLM Reasoning in Chart-to-Code Generation

Minggui He, Mingchen Dai, Jian Zhang, Yilun Liu, Shimin Tao, Pufan Zeng, Osamu Yoshie, Yuya IEIRI

- A structured intermediate representation, termed Chart Specification, is introduced for faithful chart-to-code generation.
- It shifts model training from surface-level code imitation to semantically grounded structural supervision.
- A structure-aware Spec-Align Reward is designed to provide fine-grained and verifiable feedback for reinforcement learning optimization.
- Extensive experiments on three public benchmarks demonstrate state-of-the-art performance with strong data efficiency.

Chart Specification: Structural Representations for Incentivizing VLM Reasoning in Chart-to-Code Generation

Minggui He^a, Mingchen Dai^b, Jian Zhang^a, Yilun Liu^c, Shimin Tao^b, Pufan Zeng^b, Osamu Yoshie^a and Yuya IEIRI^a

^aWaseda University, Japan

^bUniversity of Science and Technology of China, China

^cNanKai University, China

ARTICLE INFO

Keywords:

Chart to code Generation
Vision Language Models
MLLM Post-Training
RLVR

ABSTRACT

Vision-Language Models (VLMs) have shown promise in generating plotting code from chart images, yet achieving structural fidelity remains challenging. Existing approaches largely rely on supervised fine-tuning, encouraging surface-level token imitation rather than faithful modeling of underlying chart structure, which often leads to hallucinated or semantically inconsistent outputs. We propose **Chart Specification**, a structured intermediate representation that shifts training from text imitation to semantically grounded supervision. Chart Specification filters syntactic noise to construct a structurally balanced training set and supports a **Spec-Align Reward** that provides fine-grained, verifiable feedback on structural correctness, enabling reinforcement learning to enforce consistent plotting logic. Experiments on three public benchmarks show that our method consistently outperforms prior approaches. With only 3K training samples, we achieve strong data efficiency, surpassing leading baselines by up to 61.7% on complex benchmarks, and scaling to 4K samples establishes new state-of-the-art results across all evaluated metrics. Overall, our results demonstrate that precise structural supervision offers an efficient pathway to high-fidelity chart-to-code generation. Code and dataset are available at: <https://github.com/Mighten/chart-specification-paper>

1. Introduction

Charts constitute a primary medium for quantitative communication, conveying dense numerical values, structural relationships, and analytical intent across scientific literature, business intelligence dashboards, and public reports. As a result, the ability to automatically interpret and repurpose chart visualizations is a fundamental requirement for intelligent document processing systems [1]. Among related tasks, *chart-to-code generation* has recently emerged as a particularly challenging and consequential problem. Given a static raster chart image, the goal is to generate executable plotting code that faithfully reconstructs the original figure [2]. Beyond practical applications such as chart editing, reuse, and reproducibility, this task serves as a stringent test of a model's ability to recover layout structure, data mappings, and numerical relationships from visually encoded information [3].

Recent advances in Large Vision-Language Models (VLMs) suggest a promising direction for addressing this challenge. Pre-trained on large-scale image-text corpora, VLMs demonstrate strong capabilities in visual grounding and cross-modal alignment, making them natural candidates for mapping chart images to high-level plotting instructions [4]. However, despite these advances, robust chart-to-code generation remains elusive. Unlike natural images, charts encode precise and structured information, such as bar heights, line trajectories, and spatial dependencies, where

even minor errors in code can lead to significant visual discrepancies. Although recent benchmarks and datasets [5, 6] have begun to explore this problem, existing approaches still exhibit brittle generalization and persistent structural errors.

We argue that these failures are stem from a fundamental limitation of *direct chart-to-code supervision*. Charts encode information in a continuous and spatially structured visual domain, whereas plotting code is discrete, symbolic, and procedural. Directly supervising code tokens from chart images forces models to bridge this cross-domain gap in a single step, where the supervision signal is dominated by syntactic variability rather than visual or structural intent. As a result, token-level objectives provide weak guidance on which visual structures must be preserved, leading to unstable optimization and poor structural fidelity. This mismatch gives rise to three characteristic failure modes observed in existing chart-to-code systems:

First, models are prone to structural hallucinations due to the dual burden of visual reasoning and code syntax. Unlike conventional VLM tasks, chart-to-code generation requires precise interpretation of visual elements while simultaneously composing valid plotting commands. As illustrated in Figure 1, a baseline model hallucinates a dependency between independent data series, incorrectly encoding "Random Noise" as an additive component of the "Exponential Focus" trend. Although the generated code is syntactically valid, it fails to reflect the true visual semantics of the chart.

Second, the token-level prediction objective is inherently misaligned with the goal of visual fidelity. Existing

*Corresponding author

 yoshie@waseda.jp (O. Yoshie)

ORCID(s):

¹Minggui He and Mingchen Dai contributed equally to this work.

approaches, such as ChartCoder [7], primarily rely on scaling supervised training data to improve performance. However, next-token prediction treats plotting code as a sequence of text tokens, largely ignoring the visual consequences of individual commands. As a result, severe numerical or layout errors are weakly penalized as long as the generated code remains statistically plausible, preventing models from developing global structural awareness.

Third, the lack of outcome-oriented feedback limits further optimization. While recent work has explored reinforcement learning (RL) to improve executable code quality [8, 9], applying RL to chart-to-code generation exposes a critical reward gap. Binary execution feedback is overly sparse, as many structurally incorrect charts compile successfully, whereas pixel-level comparisons are unreliable due to noise from stylistic and non-structural variations. Without a verifiable and fine-grained metric that reflects structural correctness, it is infeasible to guide models toward consistent and constraint-respecting plotting logic.

To overcome these limitations, we propose **Chart Specification**, a canonical intermediate representation that explicitly encodes the structural logic of a chart. Rather than directly predicting plotting code, Chart Specification abstracts essential visual factors, such as layout composition, coordinate systems, data bindings, and functional relationships, while remaining invariant to superficial syntactic differences in code. Crucially, this representation is aligned with both the visual domain and the execution semantics of plotting libraries, enabling supervision signals to be transmitted more effectively across modalities.

Building on Chart Specification, we design two complementary components that operationalize this representation during training. First, we construct **ChartStruct**, a structurally balanced dataset that addresses the long-tail distribution hidden within coarse chart categories. By organizing samples according to fine-grained specifications, ChartStruct ensures coverage of diverse generative patterns, such as line charts defined by explicit functional mappings versus those derived from discrete interpolated data. Second, we introduce the **Spec-Align Reward**, a structure-aware metric that directly measures the agreement between generated and reference specifications. This reward provides dense, verifiable feedback suitable for reinforcement learning, effectively closing the reward gap in chart-to-code optimization.

We evaluate our approach on three public chart-to-code benchmarks. Despite using substantially fewer training samples, our method consistently outperforms prior approaches on complex benchmarks with only 3K samples, and further establishes new state-of-the-art results when scaled to 4K. These results demonstrate that Chart Specification enables models to learn the generative logic of charts with significantly improved data efficiency, reducing reliance on massive-scale supervision. Moreover, our experiments show that spec-aligned reinforcement learning substantially enhances structural fidelity and logical coherence, successfully resolving complex data dependencies that standard supervised baselines fail to capture.

The main contributions of this work are summarized as follows:

- We identify the cross-domain supervision limitation inherent in direct chart-to-code learning and propose **Chart Specification** as a structure-aware intermediate representation that bridges visual perception and code execution.
- We leverage this specification to construct **ChartStruct**, a dataset balanced by fine-grained structural categories, and design the **Spec-Align Reward**. This reward mechanism provides dense, outcome-oriented feedback, enabling effective reinforcement learning optimization.
- We achieve new state-of-the-art results across three public benchmarks, with markedly superior data efficiency. Our method surpasses prior approaches on complex metrics using only 3K training samples and sets new performance records at 4K, successfully disentangling complex data dependencies where baselines fail.

2. Related Work

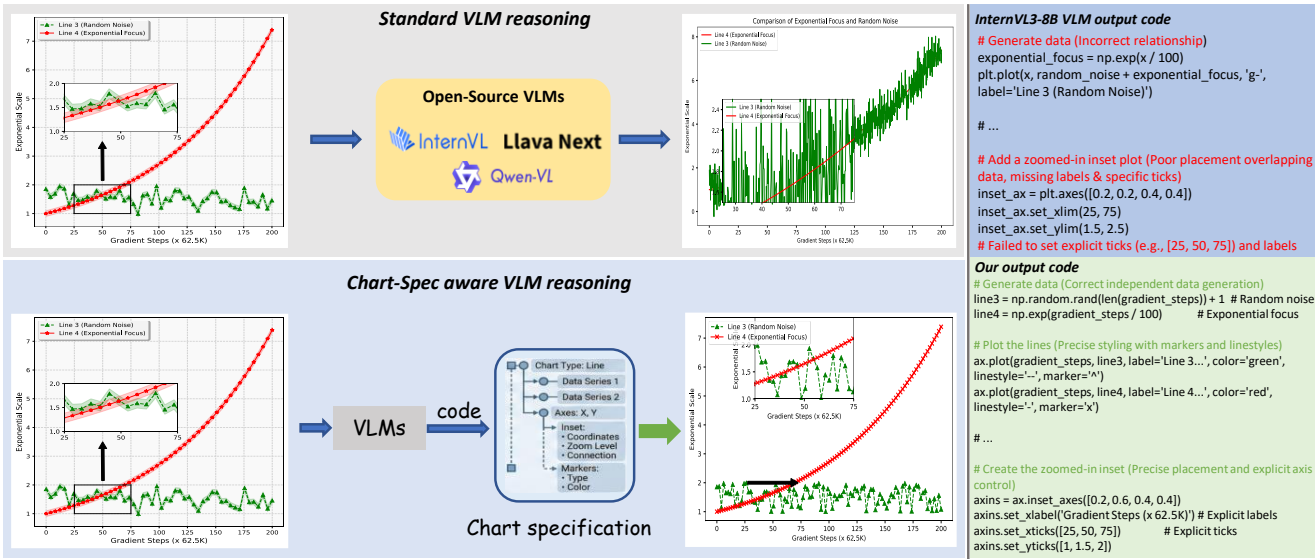
2.1. Chart-to-Code Generation

Chart-to-code generation, aiming to reconstruct executable plotting code from chart images, has evolved from early neural translation to large-scale benchmarking. Pioneering works like Pix2Code [10] and Chart2Code [11] treated this as an image-to-text problem, yet they struggled with evaluation, as standard metrics like BLEU fail to capture the logical validity of code. Subsequent studies, including Plot2Code [6] and DePlot [12], introduced larger datasets to improve generalization across plotting libraries. More recently, ChartCoder [7] scaled up the training data to 160k samples, attempting to enhance executability through massive supervised fine-tuning.

Compared with these fully supervised approaches, which often treat code as flat sequences and rely on scaling to cover corner cases, our work introduces Chart Specification as a structural intermediate representation. Instead of merely minimizing textual loss, we focus on aligning the topological structure of the generated code with the visual intent, enabling more data-efficient learning.

2.2. Visual Reasoning for Charts

Recent advances in Vision-Language Models (VLMs) have significantly advanced chart reasoning tasks. Early efforts focused on fine-tuning large-scale pre-trained models for tasks like Chart Question Answering (ChartQA). For instance, [13] apply supervised fine-tuning to extract relevant chart components for QA, while [14] extends BERT-based architectures with chart features to enhance performance. To handle more complex logic, Chain-of-Thought (CoT) methodologies have been widely adopted. Approaches such as Multimodal CoT [15] and CoT-VLA [16] break down reasoning into intermediate steps to improve decision-making.



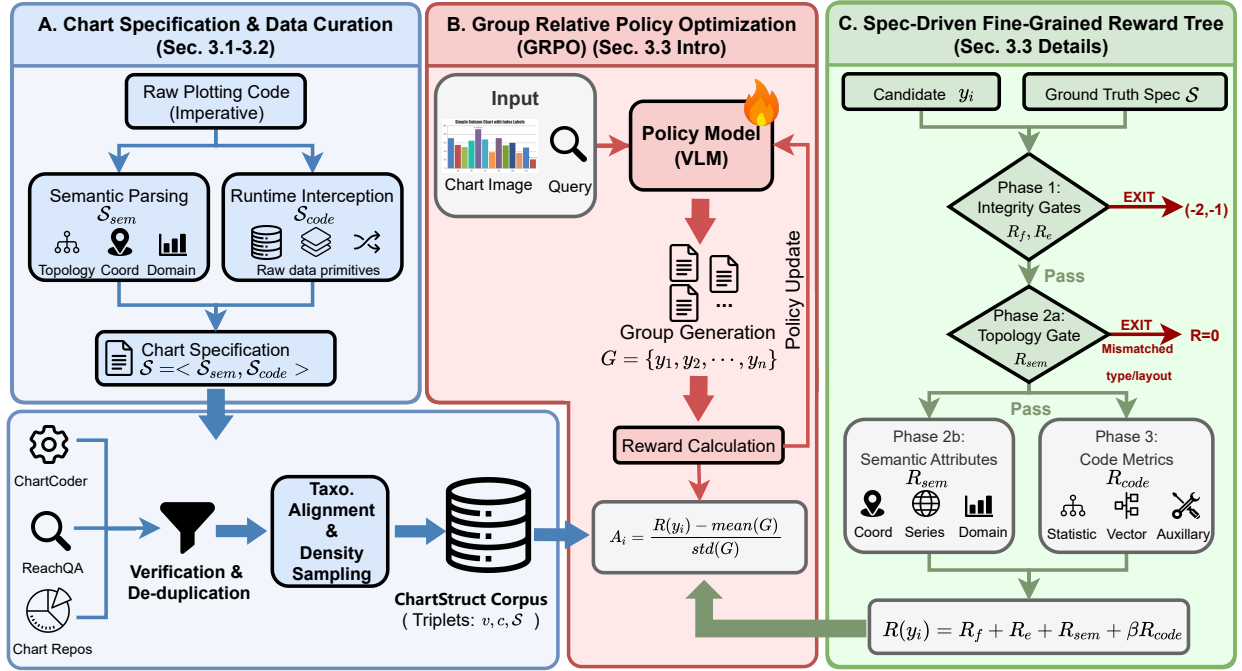


Figure 2: The Overview of Our Framework. (A) Specification-Driven Data Curation: Adopting Chart Specification (S) to extract semantic intent (S_{sem}) and physical execution data (S_{code}) from raw scripts, and guiding the curation of the ChartStruct corpus. (B) Group Relative Policy Optimization: The VLM policy is optimized using group-based advantage estimation. (C) Hierarchical Reward Tree: A fine-grained reward mechanism validates candidates through a staircase pipeline, checking Integrity (Phase 1) and Semantic Topology (Phase 2) before calculating precise Code Metrics (Phase 3).

grammars *Vega-Lite* [32]. These methods decompose visualizations into orthogonal components including data abstraction, coordinate systems, view composition, and analytic transformations. Rather than constructing a full visualization grammar, our goal is to derive a *minimal sufficient structural representation* tailored for chart code verification and reward computation. It ensures that S captures all semantic factors necessary for reconstructing chart structure, while remaining invariant to syntactic variations in plotting code.

Minimal Sufficient Structural Decomposition. Following the factorization principle of visualization grammars, we design S as a declarative and verifiable representation that collapses functionally equivalent imperative plotting scripts (e.g., Matplotlib) into a deterministic structural description of the visual state. Formally, we define S as a hybrid architecture:

$$S = \langle S_{sem}, S_{code} \rangle, \quad (1)$$

where S_{sem} captures semantic intent and S_{code} grounds numerical facts through execution. Although a single chart image may admit multiple imperative implementations, each instance in our corpus is associated with a fixed reference script; the specification abstracts away imperative syntax while preserving semantic intent, enabling consistent structural comparison across implementations.

Mapping Procedural Scripts to Semantic Intent (S_{sem}). As illustrated in Figure 3, S_{sem} (grey panels) normalizes

chart attributes into four structural dimensions: (1) *Global Topology*, capturing chart type, panel count and layout. (2) *Coordinate Systems*, identifying spatial projections such as cartesian, polar, or 3d. (3) *Data Domains*, defining axis ranges (x/y_domain) and categorical series labels. (4) *Analytic Representations*, abstracting data transformations into explicit functional forms.

For instance, the Density Chart in Figure 3 is specified by the extracted expression `np.exp(-(x-0)**2...)`, preserving analytic semantics beyond discrete samples. Notably, S_{sem} is designed to be human-verifiable by construction, with each field corresponding to a directly observable semantic attribute implied by the reference plotting code. In practice, S_{sem} is extracted from plotting scripts using a large language model Qwen3-32B with a carefully designed prompt. We further conduct manual verification on a curated set of 200 instances drawn from the candidate training corpus, covering all 20 chart types in our taxonomy (10 samples per type). For each chart type, the selected instances are visually diverse, exhibiting substantial structural variations in chart layouts and visual encodings. This manual inspection confirms that the extracted S_{sem} are stable and semantically consistent with the reference code across diverse chart structures.

Grounding Numeric via Runtime Interception (S_{code}). While S_{sem} captures high-level intent, our empirical analysis reveals that pure text-based extraction fails when chart data is implicitly computed or transformed at runtime. We

Chart Specification

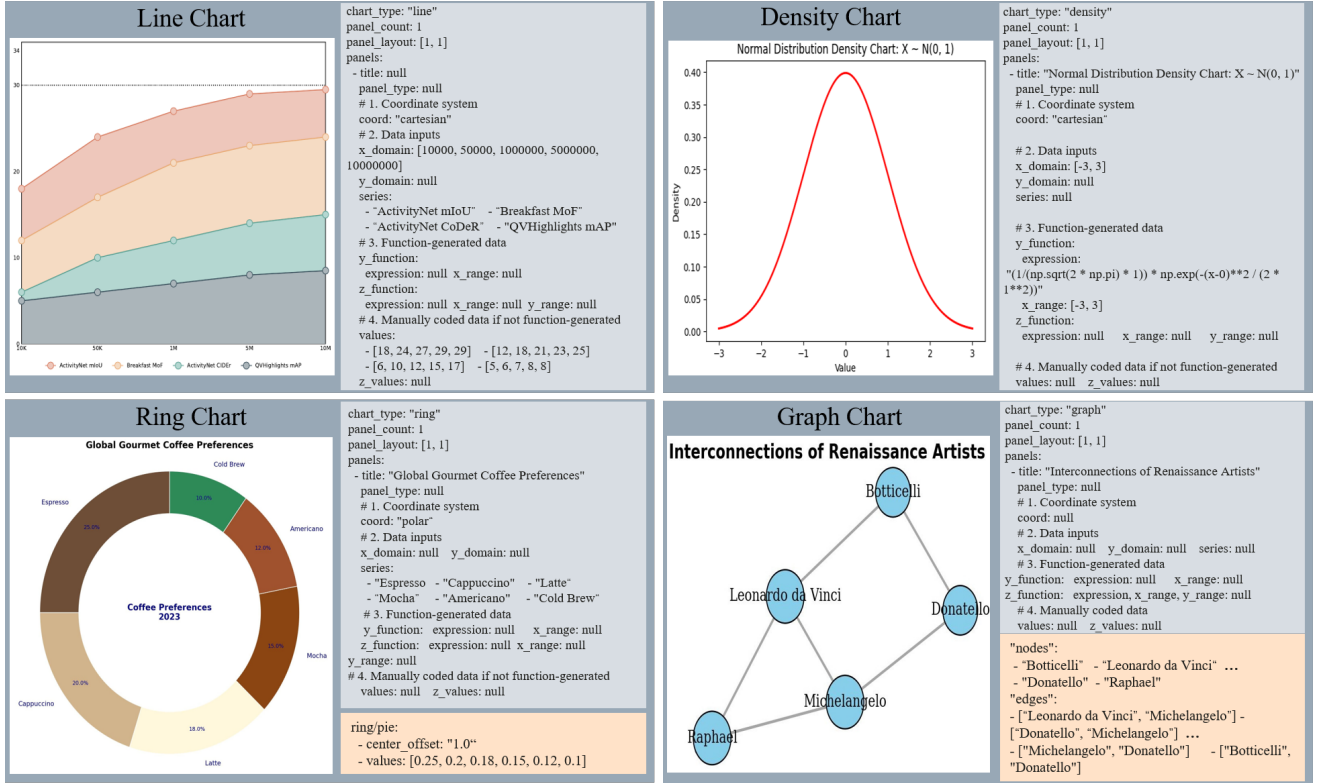


Figure 3: Visualization of our Chart Specification (S) across four distinct chart types. The grey panels represent the S_{sem} , capturing declarative intents like topology and data domains. The orange panels (bottom-left and bottom-right) illustrate the S_{code} , which uses runtime interception to capture implicit data, such as calculated wedge ratios in Ring charts or node-edge relationships in Network graphs.

address these issues by introducing S_{code} through runtime interception. By hooking into core plotting primitives (e.g., `plt.pie`, `nx.draw`), we intercept the execution stack to capture exact data primitives directly from the rendering engine. As shown by the orange panels in Figure 3, this enables recovering implicit quantities such as wedge proportions in Ring charts (e.g., `values: [0.25, 0.2, 0.18, 0.15, 0.12, 0.1]`) and explicit materialization of node-edge topology in Graph charts. Here, S_{code} is obtained via a custom Python instrumentation layer that intercepts numerical primitives during plot execution.

3.2. Curation of the ChartStruct Training Corpus

We propose ChartStruct, a spec-driven data curation pipeline for constructing structurally balanced chart-to-code corpora from large, heterogeneous plotting code repositories. Using this pipeline, we instantiate a 4K-scale corpus as the default training set for our main experiments, consisting of 3996 chart triplets $D = \{(v, c, S)\}$, where v is the chart image, c the executable code, and S the corresponding Chart Specification. The same pipeline naturally supports smaller instantiations by adjusting the target density of structural fingerprints; in particular, we construct a 3K-scale variant (3008 samples) that is used for data efficiency analysis and ablation studies.

Taxonomy Alignment and Verification. The ChartStruct curation pipeline begins by aligning raw chart data into our unified taxonomy to ensure consistency with our subsequent data curation pipeline. We curate our corpus primarily from ChartCoder [7] and consolidate its 27 chart types into 20 canonical families by merging morphologically similar variants (e.g., area into line, bubble into scatter). Each candidate sample is retained only if its code executes successfully and can be *losslessly mapped* into the Chart Specification schema. This verification stage filters the raw repository into a Spec-valid candidate pool, which serves for next topological balancing stage.

Structural Topology Tagging. With a naive inspection of the verified candidate pool, we observe a pronounced topological imbalance inherited from the raw data source. For example, in the verified ChartCoder pool, certain chart families (e.g., bar) contain over 10,000 valid samples, yet the majority differ only in surface-level numeric values while sharing identical plotting logic, obscuring the long tail of structurally distinct chart configurations. To address this issue, ChartStruct assigns high-level *structural signatures* derived from the Chart Specification to each sample, characterizing a chart's underlying topology beyond surface-level content. We define a structural signature S_{struct} as a tuple of three core dimensions: (1) *Coordinate Space* (Cartesian,

Table 1

The data distribution of a 4K instantiation for the Chart-Struct corpus. We define a target sample count per structural signature (N_{target}) based on structural complexity ($\rho \approx 90/72/54$ for Tier 1/2/3).

Family	Source Mapping	Signature	ChartCoder	Count	Ratio
		Num	Pool		
Tier 1: High Complexity (Target $\rho = 90$)					
mix	{combination, inset}	7	2878	630	15.8%
3d	{3d}	4	3045	360	9.0%
multi_axes	{multi_axes}	3	1507	270	6.8%
radar	{radar}	2	2270	180	4.5%
rose	{rose}	2	1245	180	4.5%
contour	{contour}	2	246	180	4.5%
quiver	{quiver}	2	846	180	4.5%
Tier 2: Standard Scientific (Target $\rho = 72$)					
boxplot	{boxplot}	3	2525	216	5.4%
pie	{pie}	2	2678	144	3.6%
heatmap	{heatmap}	2	2040	144	3.6%
error	{error bar}	2	922	144	3.6%
ring	{ring}	2	1549	144	3.6%
violin	{violin}	1	1627	72	1.8%
treemap	{treemap}	1	1358	72	1.8%
Tier 3: Basic Primitives (Target $\rho = 54$)					
bar	{bar, bar_num}	7	10931	378	9.5%
line	{line, area}	6	7838	324	8.1%
scatter	{scatter, bubble}	4	3967	216	5.4%
graph	{graph}	1	124	54	1.4%
histogram	{histogram}	1	651	54	1.4%
density	{density}	1	95	54	1.4%
Total		55	48342	3996	100%

Polar, or 3D); (2) *Data Mode* (Explicit Values, Analytic Functions, or Matrix Grids); and (3) *Composition Topology* (Single-series, Grouped/Stacked Multi-series, or Subplots). Enumerating these structural signatures S_{struct} across the verified pool yields 55 distinct categories spanning the 20 chart families.

Complexity-Adaptive Sampling. Following the above steps, we obtain a signature-annotated candidate pool. However, these structural signatures exhibit vastly different learning curves. Prior studies [33, 7] indicate that models struggle significantly more with complex layouts, such as 3D and nested subplots, due to the intricate spatial logic required. To address this, ChartStruct adopts a difficulty-aware sampling strategy, which allocates sampling density according to structural learning difficulty. Constrained by a target budget of 4,000 samples for training efficiency, we calibrate the target density ρ to prioritize structural difficulty over raw frequency: we allocate a higher quota ($\rho \approx 90$) to Tier 1 structures to guarantee sufficient coverage of their complex configuration spaces, while limiting basic Tier 3 families to a minimal saturation point ($\rho \approx 54$) to prevent overfitting. The detailed statistics of the resulting data distribution are reported in Table 1.

3.3. Spec-Align Fine-Grained Reward Modeling

Our reward system leverages the Chart Specification (\mathcal{S}) to provide fine-grained and structure-aware feedback. This mechanism is implemented within the Group Relative Policy Optimization (GRPO) framework [24, 25], which optimizes the policy by comparing the relative quality of

multiple responses sampled from the same prompt. To support advantage estimation in GRPO, we design a multi-stage reward mechanism that progressively differentiates superior and inferior generated code. For a group of completions $G = \{y_1, y_2, \dots, y_n\}$ generated from the same prompt, the advantage A_i for the i -th completion y_i is calculated as:

$$A_i = \frac{R(y_i) - \text{mean}(G)}{\text{std}(G)} \quad (2)$$

Here, $\text{mean}(G)$ and $\text{std}(G)$ denote the mean and standard deviation of the rewards within the group. The total reward $R(y)$ is a composite score formulated as:

$$R(y) = R_f + R_e + R_{sem} + \beta R_{code} \quad (3)$$

In this formulation, R_f , R_e , R_{sem} , and R_{code} represent the Format, Execution, Semantic, and Code rewards, respectively. As illustrated by the Reward Tree in Figure 2 and detailed in Table 2, these components are applied in a gated, staircase-like manner, where advanced structural rewards are only accessible after foundational constraints are satisfied. Importantly, reward components are conditionally instantiated based on chart semantics, rather than being uniformly applied across all chart types.

Initial Verification Phase. The first stage of the sequence establishes the basic viability of the output. Format Reward (R_f) enforces the "think-then-answer" structure by verifying reasoning tags, penalizing any attempt to skip the step-by-step reasoning phase with a score of -2 . The Execution Reward (R_e) subsequently assesses the runnability of the generated code. We assign a positive score of 0.5 for successful compilation and a penalty of -1 for syntax errors. This asymmetric design treats execution success as a filtering signal during relative ranking, distinguishing functional candidates without allowing execution to dominate downstream structural rewards.

Hierarchical Semantic Refinement (R_{sem}). The semantic-spec reward R_{sem} targets chart families whose visual intent is primarily expressed through explicit data values or analytic transformations (e.g., bar, line, scatter, heatmap). It is evaluated through a hierarchical gated process.

(1) **Topological Gate:** The system first verifies global chart topology, including chart type, panel layout, and panel count, using a binary match criterion (Table 2, Topology Gate). If this check fails, the computation of R_{sem} is terminated immediately with an early exit, yielding reward score 0 . This hard gating mechanism prevents noisy gradients from fine-grained attributes when the overall chart structure is incorrect, encouraging the model to master global organization before local details.

(2) **Detailed Attribute Alignment:** After passing the gate, R_{sem} accumulates normalized scores in $[0, 1]$ for panel-level attributes, including coordinate systems (Coord), axis or

Table 2

Hierarchical reward components and fine-grained scoring criteria used for Spec-Align reward modeling. The reward is organized into integrity checks, semantic structure alignment (R_{sem}), and code-level fidelity (R_{code}).

Component	Metric	Description	Score (R)
Integrity Checks			
Format (R_f)	Binary Match	Think-then-Answer structure verification.	{0, -2}
Execution (R_e)	Compilation	Compilation check in sandbox.	{0.5, -1}
Semantic-Spec Reward (R_{sem})			
Topology Gate	Binary Match	Global chart structure consistency: chart type, panel layout, and panel count.	Pass / {3}
Coord	Match	Classification of coordinate system (e.g., Cartesian, polar, 3D).	[0, 1]
Domain	Range IoU	Overlap of axis ranges or categorical domains.	[0, 1]
Series	Jaccard	Consistency of legend labels and grouping sets.	[0, 1]
Data / Func	Edit Dist. / MSE	Formula string matching or numeric sample error.	[0, 1]
Code-Spec Reward (R_{code})			
Statistical	L_2 Distance	Boxplot quartiles or violin envelope statistics.	[0, 1]
Relational	F1-Score	Treemap area ratios or graph node-edge relations.	[0, 1]
Vector	Cosine Sim.	Vector field direction and magnitude alignment.	[0, 1]
Auxiliary	Edit Dist.	Text annotations, spatial positions, event markers, or color consistency.	[0, 1]

categorical domains (Domain), legend and grouping consistency (Series), and data values or analytic expressions (Data / Func).

Notably, the Data/Function component is instantiated only when raw values or analytic expressions are explicitly defined in the chart specification. For chart families such as boxplots or violins, whose semantics are conveyed through derived statistics, this component is intentionally left Null.

Fine-Grained Numerical Calibration (R_{code}). Complementing to R_{sem} , the code-spec reward R_{code} provides implementation-level feedback for chart families whose semantics are not fully captured by value- or function-level alignment but instead depend on statistical, relational, or geometric properties. Its components are selectively activated by chart family, avoiding conflicting or redundant supervision. Specifically, R_{code} instantiates four chart-family-specific metrics in Table 2, computed from the runtime code-spec schema.

(1) Statistical. For boxplots, we extract per-category statistics (min, q1, median, q3, max) from predicted and reference executions and compute an L_2 distance over the concatenated statistic vectors; for violins, we compute the L_2 distance between envelope summaries (e.g., min/median/max and/or sampled boundary points). The distance is converted to a bounded score in [0, 1] via a monotonic normalization. (2) Relational. For treemaps, we compare normalized area ratios of leaf nodes and score them by F1 based on a tolerance-aware match between predicted and reference leaves; for graphs, we compute F1 over recovered edge sets (and node/label sets when available) under canonicalized node identities. (3) Vector. For quiver plots, we extract vector components ($\Delta x, \Delta y$) at corresponding anchors and compute cosine similarity of directions (optionally weighted by magnitude); for contour

plots, we compare recovered level sets (or level values when only levels are available) using set similarity. (4) Auxiliary. For text and annotations, we compute edit distance on string content and Euclidean distance on normalized positions; for color, we compare color assignments under canonicalized palettes or label-aligned mappings. All metrics are normalized to [0, 1] for comparability.

These code-level rewards are mutually exclusive with semantic data-level components and are normalized to [0, 1] for numerical comparability. The weighting coefficient $\beta = 0.5$ mediates the relative influence of semantic abstraction (R_{sem}) and implementation fidelity (R_{code}), enabling a controlled transition between abstraction regimes rather than balancing competing signals on the same attributes.

4. Experiments settings

4.1. Implementation Details

We adopt Qwen2.5-VL-7B [34] as the backbone model, chosen for its strong visual understanding capability and parameter efficiency [35]. Unless otherwise specified, all main experiments are trained on the 4K-scale ChartStruct instantiation described in Sec. 3.2, while a 3K-scale variant (3,008 samples) is used for ablation studies due to computational constraints.

We fine-tune the full parameters of the language model and the vision-language projector using Group Relative Policy Optimization (GRPO) [24], while keeping the visual encoder frozen to preserve pre-trained visual features. Training is conducted for 3 epochs with a learning rate of 4×10^{-7} and a global batch size of 32. During exploration, we sample 16 rollouts per update to estimate group advantages, and set both prompt and response length limits to 3,000 tokens. The KL divergence coefficient is fixed at 0.001 for training

stability. All experiments were run on 8 NVIDIA A100 (80GB) GPUs, completing in approximately 62 hours.

4.2. Benchmarks and Evaluation Metrics

We utilize three complementary benchmarks to evaluate the model’s chart understanding and code generation capabilities across different domains and difficulty levels.

ChartMimic [5] focuses on evaluating the ability of MLLMs to redraw publication-quality charts from ArXiv papers, focusing on the strict preservation of the original style and visual appearance. Following the official settings, we adopt the Direct Mimic task for evaluation on a test subset of 600 samples. We report the Execution Rate to assess code validity, alongside Low-Level metrics which compare specific code attributes (e.g., layout, color, text) against the ground truth to measure structural fidelity. In addition, High-Level scores are computed by GPT-4o to assess the overall visual similarity.

Plot2Code [6] serves as a standard testbed for programmatic visualization skills, aiming to convert figures from Matplotlib galleries into executable code. We evaluate models on the Direct Asking task using the standard test set of 132 samples. Performance is assessed using three metrics: Pass Rate for executability, Text-Match for token-level similarity, and a model-based Rating (via GPT-4o) to comprehensively judge the visual chart quality of the generated code.

ChartX [13] constitutes a large-scale benchmark covering a diverse distribution of general chart types and visual styles. To evaluate generalization capabilities beyond scientific figures, we select the Redrawing task and conduct evaluations on the test set of 1,152 samples. We report the GPT-Score evaluated by GPT-4o to measure the semantic consistency between the generated chart and the user instructions.

4.3. Baseline Methods

We compare our method against a comprehensive set of Multimodal LLMs (MLLMs). To ensure a fair and rigorous evaluation, we categorize these baselines into three distinct groups based on their accessibility and training domain:

Commercial MLLMs. We include the commercial models reported in the official benchmark leaderboards to serve as high-performance references. This selection includes GeminiProVision [36], Claude-3-Opus [37], GPT-4V [38], and GPT-4o [39]. These models provide the standard upper-bound performance metrics established in the respective benchmark papers.

Open-Source MLLMs. We include a wide range of top-tier generalist MLLMs. Specifically, we evaluate the InternVL2 series (4B, 8B, 26B, 76B) [40], Qwen2-VL (7B, 72B) [34], DeepSeek-VL-7B [41], LLaVA-Next [42], and MiniCPM-Llama3-V2.5 [43]. Note that while our method is built on Qwen2.5-VL-7B [34], we mainly compare against

these standard baselines to maintain consistency with the existing literature.

Chart-Domain MLLMs. To contrast our structural reinforcement strategy with existing specialized approaches, we compare against models explicitly fine-tuned for chart-to-code generation tasks. This category includes ChartLlama [33], ChartAssistant [44], TinyChart [45], ChartVLM [13] and ChartCoder[7].

5. Experimental Results

In this section, we present the empirical evaluation of ChartSpec. We first report comparative results against relevant baselines across the three benchmarks, followed by ablation studies that analyze the contributions of our data construction and reinforcement learning strategies.

5.1. Evaluation on ChartMimic

We first evaluate performance on ChartMimic, with quantitative results summarized in Table 3. Our ChartSpec achieves leading performance among open-source MLLMs. Even with the standard 3k training set, it attains an Overall Score of 79.9, outperforming the previous specialist leader, ChartCoder (75.7). Scaling to 4k boosts the score to 82.4, significantly surpassing large-scale generalists like InternVL2-Llama3-76B (58.5). This demonstrates that our spec-driven alignment is highly data-efficient, yielding dominant performance without requiring massive pre-training scale.

Furthermore, ChartSpec exhibits exceptional competitiveness against top-tier proprietary models. Most notably, our 4k model surpasses GPT-4o (81.2) with a score of 82.4, while maintaining a substantial lead over Claude-3-Opus and GeminiProVision. This result confirms that a compact 7B model, when equipped with precise structural supervision, can rival or exceed the capabilities of commercial giants in domain-specific tasks.

A detailed breakdown reveals the robustness of this performance. Unlike ChartCoder, which excels in Layout (95.0) but degrades significantly in Text rendering (67.2), ChartSpec achieves a superior balance. Our model maintains a high Layout score of 92.8 while simultaneously securing a Text score of 80.5, comparable to GPT-4o. Finally, our method achieves the highest Execution Rate of 93.5% on the leaderboard, confirming that the Spec-Align reward effectively minimizes syntax errors and runtime failures.

5.2. Evaluation on Plot2Code and ChartX

To further assess the capability of ChartSpec on unseen data distributions, we extend our evaluation to the Plot2Code and ChartX benchmarks.

Performance on Plot2Code As shown in Table 4, ChartSpec demonstrates exceptional robustness on the Plot2Code benchmark. Most notably, our model achieves a **Pass Rate of 88.7%**, effectively surpassing top-tier proprietary models including GPT-4o (88.6%) and Claude-3-Opus (84.1%).

Table 3

Main results on the **ChartMimic** benchmark comparing ChartSpec against leading proprietary and open-source models. The evaluation covers code executability, low-level visual fidelity (Text, Layout, Type, Color), and high-level visual assessment.

Models	Para.	Exec. Rate	Low-Level					High-Level	Overall	
			Text	Layout	Type	Color	Avg.			
Full score	-	100	100	100	100	100	100	100	100	
<i>Commercial MLLMs</i>										
GPT-4o	-	93.2	81.5	89.8	77.3	67.2	79.0	83.5	81.2	
Claude-3-opus	-	83.3	66.8	83.1	49.9	42.1	60.5	60.1	60.3	
GeminiProVision	-	68.2	52.6	64.2	51.3	47.1	53.8	53.3	53.6	
<i>Open-Source General-Domain</i>										
InternVL2-2B	2.2B	52.5	23.6	35.8	16.0	15.4	22.7	24.2	23.5	
InternVL2-4B	4.2B	66.2	34.7	51.7	25.2	23.6	33.8	38.4	36.1	
InternVL2-8B	8.1B	61.8	31.5	51.1	28.6	26.2	34.4	38.9	36.6	
InternVL2-26B	26.0B	69.3	39.2	58.7	35.9	31.8	41.4	47.4	44.4	
InternVL2-Llama3-76B	76.0B	83.2	54.1	74.5	49.2	41.5	54.8	62.2	58.5	
MiniCPM-Llama3-V-2.5	8.4B	80.3	30.7	49.6	38.6	27.6	36.6	42.1	39.4	
LLaVA-Next-Mistral-7B	7.6B	59.7	14.0	31.1	19.8	17.8	20.7	21.3	21.0	
LLaVA-Next-Yi-34B	34.8B	50.2	15.9	29.6	17.6	15.2	19.6	20.6	20.1	
DeepSeek-VL-7B	7.3B	41.3	15.3	26.6	19.7	14.5	19.0	20.4	19.7	
Qwen2-VL-7B	8.2B	67.0	26.4	51.0	31.0	23.3	32.9	35.0	34.0	
Qwen2-VL-2B	2.6B	47.0	20.1	29.5	21.3	17.9	22.2	23.4	22.8	
Qwen2.5-VL-7B(backbone)	7B	69.2	52.0	77.2	74.3	47.1	62.7	63.2	63.0	
<i>Open-Source Chart-Domain</i>										
ChartLlama	13B	57.5	-	-	-	-	24.8	28.1	26.5	
TinyChart	3B	42.5	-	-	-	-	26.3	25.9	26.1	
ChartVLM-L	14.3B	83.2	-	-	-	-	15.8	13.9	14.9	
ChartCoder	7B	91.4	67.2	95.0	78.5	69.0	77.4	74.0	75.7	
ChartSpec(Ours) + 3k	7B	90.2	73.7	90.7	83.7	65.7	78.4	81.4	79.9	
ChartSpec(Ours) + 4k	7B	93.5	80.5	92.8	82.0	67.0	80.6	84.2	82.4	

This result is particularly significant given the parameter disparity; ChartSpec (7B) outperforms the massive open-source generalist InternVL2-Llama3-76B (85.6%) by a clear margin. In terms of code quality, our model achieves a Text-Match score of 55.3, which is competitive with GPT-4o (56.3) and significantly higher than other 7B evaluations such as DeepSeek-VL (32.6) and Qwen2-VL (33.8). This confirms that our Spec-Align reward does not merely optimize for visual similarity but also ensures high semantic fidelity in the generated code.

Performance on ChartX The results on ChartX further validate the structural versatility of our approach. ChartSpec establishes a new state-of-the-art with an overall GPT-score of 3.52, outperforming GPT-4V (2.63) and the previous best chart specialist, ChartCoder (2.09), by a substantial margin. To understand the source of this superiority, we provide a detailed type-wise breakdown in Table 5. While baseline models typically exhibit performance degradation on fine-grained or complex chart types, ChartSpec maintains consistent high performance across the board. For instance, on geometrically complex categories such as *Radar* and

Bubble charts, our model scores 3.30 and 3.52 respectively, whereas GPT-4V only achieves 2.30 and 2.40. This indicates that our model has internalized a generalized understanding of visual plotting logic, allowing it to handle diverse topological requirements that challenge even much larger vision-language models.

5.3. Ablation Study

To systematically validate our core contributions and dissect the mechanisms behind the performance gains, we conduct ablation studies along four dimensions: (1) We compare different data scales of SFT and Spec-Align RL to validate our claim that structural supervision offers superior sample efficiency compared to surface-level pattern imitation. (2) We analyze the positive effect of the Chart Specification in data construction pipeline by comparing it with random corpus curation. (3) We decompose the Spec-Align reward components across model scales to demonstrate how fine-grained signals outperform generic objectives. (4) Finally, we investigate the optimal utilization of the Spec-Align reward. Specifically, we compare direct policy

Table 4

Comparison of Model Performance on Plot2Code and ChartX. All results are taken directly from the official Plot2Code[6] and ChartCoder[7] evaluations.

Models	Params	Plot2Code			ChartX
		Pass Rate	Text-Match	Rating	GPT-score
Full score	-	100	100	10	5
<i>Commercial MLLMs</i>					
GeminiProVision	-	68.2	53.6	5.06	-
Claude-3-opus	-	84.1	57.5	4.37	-
GPT-4V	-	84.1	57.7	6.48	2.63
GPT-4o	-	88.6	56.3	5.71	-
<i>Open-Source General-Domain</i>					
DeepSeek-VL-7B	7.3B	64.4	32.6	3.69	-
LLaVA-Next-Mistral-7B	7.6B	72.0	38.7	3.06	-
InternVL2-8B	8.1B	77.3	37.1	2.78	1.63
InternVL2-26B	26.0B	81.3	43.1	3.42	1.70
InternVL2-Llama3-76B	76.0B	85.6	46.6	3.89	1.74
MiniCPM-Llama3-V2.5	8.4B	76.3	37.3	2.61	1.66
Qwen2-VL-7B	7.0B	68.2	33.8	3.10	1.50
Qwen2-VL-72B	72.0B	72.0	53.4	4.26	1.69
Qwen2.5-VL-7B(backbone)	7.0B	73.5	47.1	4.71	2.23
<i>Open-Source Chart-Domain</i>					
ChartLlama	13B	58.4	40.3	2.32	0.94
ChartAssistant	13B	-	-	-	0.82
TinyChart	3B	43.2	44.6	2.19	1.89
ChartVLM-L	14.3B	-	-	-	1.58
ChartCoder	7.0B	87.9	54.5	4.50	2.09
ChartSpec (Ours) + 3k	7B	86.4	50.3	6.28	3.38
ChartSpec (Ours) + 4k	7B	88.7	55.3	6.32	3.52

alignment against reasoning-enhanced generation to determine which paradigm better maximizes the potential of our reward mechanism.

5.3.1. Impact of Training Data Scale

We evaluate the impact of training data scale on model performance by comparing how SFT and Spec-Align RL respond to increasing data under the same data construction pipeline, and how these differences manifest in generalization behavior.

Sample Efficiency and Scaling Laws As illustrated in Figure 4, the two training paradigms exhibit fundamentally different scaling behaviors. SFT suffers from an initial performance regression. At the 1K data regime, the Pass Rate on ChartMimic drops significantly to 46.5%, falling well below

the Base model’s 69.2%. Even as the data scale increases to 4K, SFT only recovers to 67.8%, struggling to surpass the original pre-training baseline. This implies that standard SFT consumes substantial capacity re-learning low-level patterns, making it data-inefficient for this task. In contrast, Spec-Align RL demonstrates exceptional sample efficiency. With only 1K samples, it achieves an 83.0% Pass Rate, outperforming the best SFT result by a margin of 15.2%. Performance improves rapidly at 3K (reaching 90.2%) before showing signs of saturation at 4K. This confirms that the structured reward signal enables the model to grasp generative rules much faster than surface-level supervision.

Structural Generalization vs. Degradation To understand the source of this efficiency gap, we analyze the type-wise performance in Figure 5. The breakdown reveals that

Table 5

Type-wise accuracy for chart re-drawing on ChartX evaluated using GPT-score. All reported scores of baselines are obtained from the ChartX benchmark [46].

Models	General Chart Types										Fine-grained Chart Types										Avg.
	bar	bar_num	line	line_num	pie	ring	box	hist	treemap	rose	area	3D-bar	bubble	multi	radar	heatmap	funnel	candle			
QWen-VL	0.89	0.60	0.80	1.30	1.25	1.10	0.80	0.80	0.80	1.10	0.60	1.10	0.90	0.60	0.50	0.50	0.70	0.70	0.70	0.86	
SPHINX-V2	1.00	1.75	1.60	1.65	1.80	0.50	0.40	1.60	0.60	1.10	0.20	0.50	0.40	0.20	0.00	0.50	0.30	0.20	0.96		
ChartLlama	1.16	1.05	0.90	1.15	1.80	0.70	0.80	1.00	1.00	0.70	0.70	1.10	0.70	0.40	0.50	1.00	0.70	0.30	0.94		
ChartAst	0.95	1.35	0.00	0.60	0.30	0.00	1.50	2.40	0.60	1.70	1.80	0.60	0.60	1.20	0.00	0.00	2.10	0.00	0.82		
LLaVA-1.5	0.95	0.75	0.80	0.95	0.90	0.60	0.60	0.80	0.70	1.00	0.60	0.80	0.90	0.40	0.60	0.70	0.50	0.50	0.75		
GPT-4V	2.05	2.70	2.05	2.75	3.55	3.40	2.00	2.70	2.70	2.80	2.20	2.70	2.40	2.80	2.30	3.20	3.50	1.60	2.63		
ChartVLM-B	1.63	1.50	1.70	1.65	1.90	1.10	1.90	1.10	0.40	1.20	0.80	1.00	1.70	1.30	0.80	1.20	1.00	1.10	1.36		
ChartVLM-L	1.53	1.85	1.85	1.70	2.75	1.90	1.40	1.20	0.90	1.00	1.10	1.60	1.30	1.50	0.80	1.90	1.20	1.10	1.58		
ChartSpec + 3k	3.50	3.48	3.84	3.83	3.79	3.64	3.27	3.59	2.38	1.99	3.79	2.74	3.34	3.41	3.41	3.57	3.25	2.45	3.38		
ChartSpec + 4k	3.43	3.52	4.11	4.11	4.22	3.83	3.61	3.79	1.80	2.47	3.83	3.17	3.52	3.35	3.30	3.49	3.28	2.76	3.52		

— Base SFT Spec-Align RL

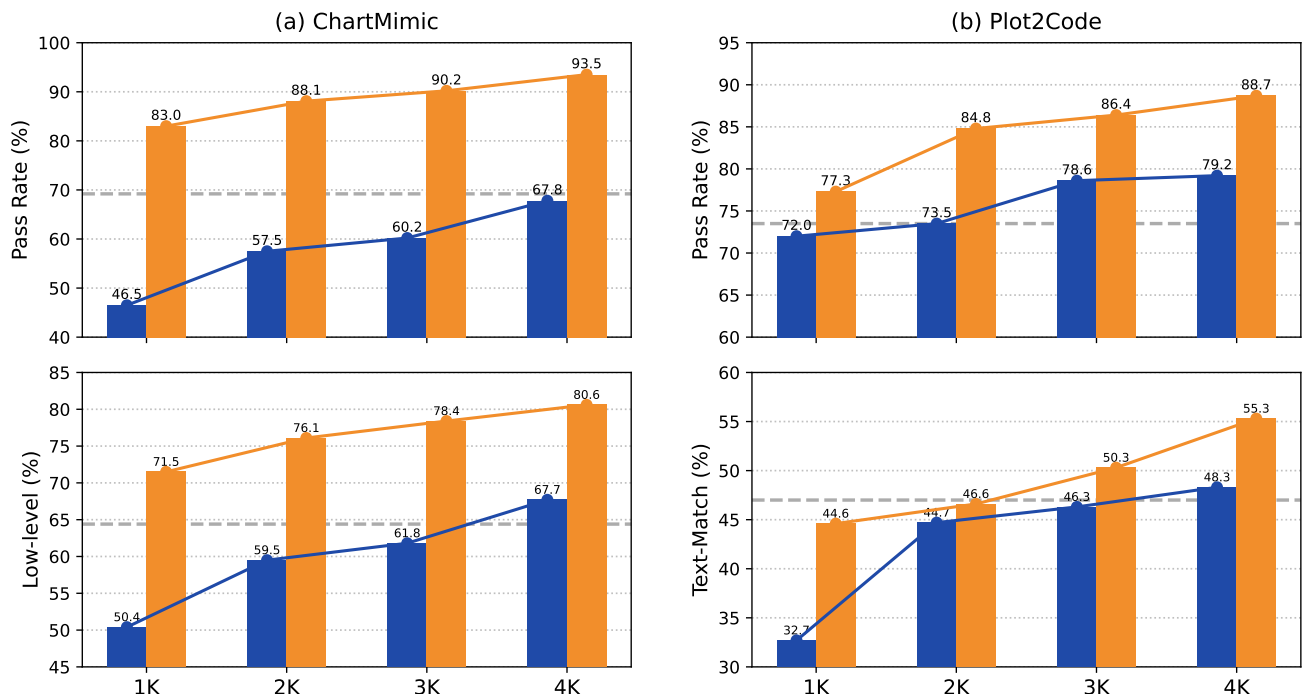


Figure 4: Impact of training data scale on chart-to-code performance. We compare SFT and Spec-Align RL across varying data sizes on ChartMimic (a) and Plot2Code (b), evaluated using Pass Rate, Low-level accuracy, and Text-Match.

SFT is prone to structural degradation in complex chart types. Although it maintains competence on standard formats, performance drops below the baseline on intricate geometries like *Contour* ($66.1 \rightarrow 48.2$) and *Violin* plots ($42.2 \rightarrow 32.8$). This suggests that SFT tends to forget the coordinate mapping logic required for complex topologies. Conversely, Spec-Align RL ensures robust generalization. Not only reverses this degradation, it achieves dominant performance in these long-tail categories, raising *Violin* scores to 69.1 and *Graph* to 78.0. This indicates that the Spec-Align reward encourages the internalization of generalized plotting logic rather than overfitting to simple, high-frequency patterns.

5.3.2. Role of Chart Spec in Data Construction

We analyze the role of Chart Specification in data construction by comparing our spec-driven ChartStruct pipeline against a baseline trained on randomly curated data. Both strategies are applied to the 3K data scale and evaluated on Qwen2-VL and Qwen2.5-VL backbones.

As presented in Table 6, the results highlight a critical distinction between code executability and semantic fidelity. The model trained on ChartStruct demonstrates superior capability in grounding generated code to the underlying data. Specifically, on the Plot2Code benchmark, the *Text-Match* score significantly improves from 48.5 to 50.3 for Qwen2.5-VL-7B and from 37.7 to 41.7 for Qwen2-VL-7B.

Chart Specification

	3d	CB	HR	PIP	area	bar	box	contour	density	errorbar	errorpoint	graph	heatmap	hist	line	multidiff	pie	quiver	radar	scatter	tree	violin	Overall
Base	61.5	69.3	45.9	65.1	79.2	73.2	52.9	66.1	53.3	72.2	72.0	73.6	49.2	60.3	79.9	58.4	62.7	54.3	55.6	71.8	53.3	42.2	64.8
SFT	49.3	58.3	44.8	53.9	77.5	67.0	63.6	48.2	44.4	65.8	70.5	65.5	49.9	44.9	75.0	65.0	75.6	45.8	50.5	77.1	89.8	32.8	61.8
RL (no-CoT)	61.7	79.3	54.9	64.0	95.2	86.3	75.9	73.5	65.3	81.3	81.6	72.3	58.8	82.0	86.3	74.6	89.1	71.4	69.3	89.6	84.6	64.4	77.3
RL (CoT)	63.9	78.8	62.2	66.6	94.1	86.6	77.4	74.4	67.0	80.3	83.5	78.0	62.2	81.4	83.9	73.1	88.9	68.3	82.5	86.5	89.7	69.1	78.4

Figure 5: Type-wise performance comparison at the 3K data scale on Chartmimic. Here, low level average accuracy across different chart types. Columns correspond to chart categories, and rows denote different training settings: **Base** (Qwen2.5VL-7B-Instruct), **SFT** (Standard Fine-Tuning), **RL (no-CoT)** (Spec-Align RL without reasoning), and **RL (CoT)** (Spec-Align RL with reasoning). The Overall column reports weighted averages over chart types.

Table 6

Ablation study on data curation strategies. Comparison between Random Curation and our Spec-Driven ChartStruct.

Model	ChartMimic		Plot2Code	
	Pass	Low	Pass	Text
Qwen2-VL-7B (Random)	88.2	72.9	88.3	37.7
+ChartStruct (Ours)	91.7	73.8	92.4	41.7
Qwen2.5-VL-7B (Random)	90.8	76.6	87.1	48.5
+ChartStruct (Ours)	90.2	78.4	86.4	50.3

A similar trend is observed on ChartMimic, where the *Low-Level* metric consistently favors the Spec-driven models, exemplified by an increase from 76.6 to 78.4 on the Qwen2.5-VL backbone. These metrics indicate that training on spec-verified data effectively forces the model to attend to precise coordinate mappings rather than hallucinating plausible but incorrect values.

This improvement in semantic precision accompanies an interesting observation regarding the Pass Rate, where minor fluctuations are observed on the Qwen2.5-VL backbone. Specifically, the Spec-driven model achieves a Pass Rate of 90.2% on ChartMimic and 86.4% on Plot2Code, both of which are marginally lower than the Random baselines (90.8% and 87.1%, respectively). We attribute this slight and consistent decrease to differences in data difficulty induced by spec-driven curation rather than reduced executability or training instability. The Random baseline is more likely to be biased toward simpler, standard chart patterns that compile easily, whereas ChartStruct enforces a balanced inclusion of diverse and structurally complex topologies. Importantly, this modest fluctuation contrasts with the substantial and consistent gains in Text-Match and Low-Level metrics, indicating that spec-driven curation shifts the model away from surface-level memorization toward structurally faithful and semantically grounded generation.

5.3.3. Efficacy and Decomposition of Reward Mechanisms

We examine the reward mechanism from two perspectives: the overall efficacy of the Spec-based RL paradigm

Table 7

Ablation study of different training strategies across various model scales (+Spec denotes our method).

Model	ChartMimic		Plot2Code	
	Pass	Low	Pass	Text
Q2.5-VL-7B	69.2	64.4	73.5	47.1
Q2.5-VL-7B+SFT	55.7	61.8	67.4	31.6
Q2.5-VL-7B+Spec	90.2	78.4	86.4	50.3
Q2.5-VL-3B	55.0	50.7	75.8	37.0
Q2.5-VL-3B+SFT	48.0	56.6	57.6	35.7
Q2.5-VL-3B+Spec	89.2	69.3	84.8	42.1
Q2-VL-7B	64.8	51.4	68.2	33.8
Q2-VL-7B+SFT	53.7	59.7	68.9	32.6
Q2-VL-7B+Spec	91.7	73.8	92.4	41.7
Q2-VL-2B	43.3	39.3	78.0	30.7
Q2-VL-2B+SFT	37.0	47.2	59.8	23.9
Q2-VL-2B+Spec	94.5	57.0	90.9	31.2

across varying model scales, and the individual contributions of semantic versus code-level specifications.

Efficacy of Spec-Based Reward Mechanisms To demonstrate the effectiveness and broad generalizability of our approach, we conduct extensive experiments across multiple model families (Qwen2-VL, Qwen2.5-VL) and varying parameter scales (2B, 3B, 7B). We compare three settings: the vanilla Base model, Supervised Fine-Tuning (SFT), and our Spec-based RL (+Spec).

The results in Table 7 reveal a compelling insight: Supervised Fine-Tuning (SFT) alone is insufficient and often detrimental for this task. Across almost all evaluated models, applying SFT leads to a drop in Pass Rate compared to the Base model (e.g., Q2.5-VL-7B drops from 69.2% to 55.7% on ChartMimic). This phenomenon suggests that standard SFT may cause the model to overfit to specific text formats while losing the precise reasoning logic required for plotting. In sharp contrast, our Spec-based RL consistently reverses this trend and achieves state-of-the-art performance. The Q2.5-VL-7B model sees a massive jump to 90.2% Pass Rate with our method. Furthermore, the improvements are

Table 8

Ablation study of different specification components on Qwen2.5-VL-7B.

Model	ChartMimic		Plot2Code	
	Pass	Low	Pass	Text
Q2.5-VL-7B (Base)	69.2	64.4	73.5	47.1
Semantic Spec Only	81.2	67.0	84.1	37.1
Code Spec (Full)	90.2	78.4	86.4	50.3

highly scalable; even the smaller Q2-VL-2B model achieves a remarkable 94.5% Pass Rate on ChartMimic with our framework, outperforming the base 7B models. This demonstrates that our reward mechanism provides a generalized solution for chart-to-code tasks, independent of the underlying backbone architecture.

Decomposition of Reward Components To further dissect the source of these gains, we analyze the specific contributions of Semantic Specifications versus Code Specifications. We use the Qwen2.5-VL-7B model as the baseline and incrementally introduce the reward components.

As illustrated in Table 8, the baseline Qwen2.5-VL-7B model exhibits a notable deficit in structural precision. The augmentation with Semantic Specifications alone primarily enhances the model’s understanding of chart types and layouts. However, the integration of full Code Specifications yields the most substantial enhancement in execution-based Pass Rate and Text-Match scores. This improvement underscores the role of explicit data descriptors in mitigating semantic hallucinations and facilitating more accurate textual anchoring within the visual field, ensuring that the generated code is not only visually similar but numerically precise.

5.3.4. Impact of Reasoning Process

We investigate the necessity of the intermediate reasoning stage by questioning whether the Spec-Align reward alone suffices for direct code generation or if an additional reasoning step is required to maximize performance.

Breaking the Performance Ceiling Table 9 provides a detailed comparison of the two training paradigms. The model trained with Spec-driven RL but without reasoning steps already achieves a substantial improvement over the baseline, increasing the Pass Rate by 19.3%. This proves that the reward signal itself is highly effective at teaching the model the general syntax of plotting code. However, this direct generation approach eventually hits a performance plateau, particularly on metrics demanding high precision. Incorporating the reasoning process allows the model to break this ceiling. This is most evident on the Plot2Code benchmark, where the reasoning model achieves a clear gain in Text-Match score (rising from 47.4 to 50.3). This improvement suggests that the intermediate reasoning tokens help the model accurately calibrate fine-grained details, such as specific color codes and legend positioning, which the direct model often fails to ground accurately.

Table 9

Ablation study on the impact of the reasoning process. *w/o Thinking* refers to the model trained to generate code directly, while *w/ Thinking* incorporates the intermediate reasoning chain.

Model Variant	ChartMimic		Plot2Code	
	Pass	Low	Pass	Text
Q2.5-VL-7B (Base)	69.2	64.4	73.5	47.1
<i>RL w/o Thinking</i>	88.5	77.3	85.8	47.4
<i>RL w/ Thinking</i>	90.2	78.4	86.4	50.3

Handling Structural Complexity To further understand where reasoning is most beneficial, we analyze the performance gains across different chart categories in Figure 5. The results show that the impact of reasoning is highly dependent on chart complexity. For standard chart types like Bar or Line plots, the performance gap between the two variants is negligible. This implies that direct visual-to-code mapping is sufficient for explicit and simple layouts. In contrast, the benefits of reasoning become dominant in structurally complex categories. We observe significant improvements in Tree and Violin plots, where the Pass Rate increases by 5.1% and 4.7% respectively. These findings confirm that while direct generation handles standard patterns well, the reasoning chain provides a necessary buffer to decompose intricate topological relations before implementation, effectively resolving ambiguities in complex geometries.

5.4. Analysis and Discussion

To intuitively evaluate generation quality, we visualize comparisons between *ChartSpec* and representative baselines in Figure 6. The results demonstrate a distinct hierarchy of capability: while standard open-source VLMs (e.g., Qwen2.5, InternVL3) suffer from catastrophic structural failures—evident in the distorted grids of the Radar Chart (Row 2) or the blank outputs in the Boxplot—our model successfully activates dormant coding capabilities to reconstruct these complex topologies. Crucially, our method closes the gap with proprietary SOTA models, achieving visual alignment comparable to GPT-4o, particularly in the layout precision of the Area Chart (Row 1). Most notably, our approach exhibits superior statistical rigor in fine-grained details; in the Boxplot scenario (Row 3), while GPT-4o generates a visually smooth approximation that omits data nuances, our model leverages runtime interception (S_{code}) to accurately render the outlier points (small circles), confirming that our spec-driven reward mechanism prioritizes mathematical fidelity alongside visual imitation.

6. Conclusion

In this paper, we introduced a verifiable reinforcement learning framework to bridge the gap between visual perception and code generation. By shifting from textual code

Chart Specification

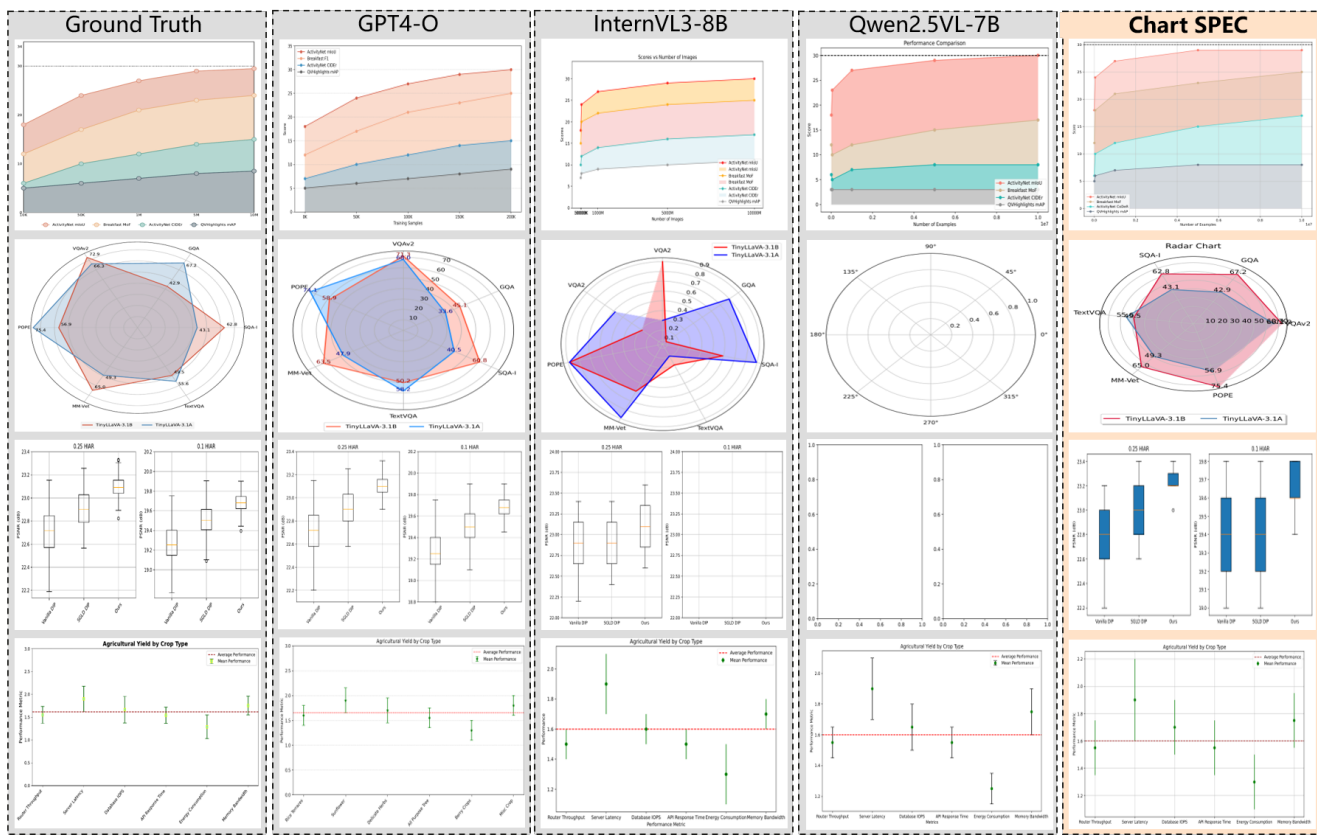


Figure 6: Qualitative comparison on the ChartMimic validation set. **Left to Right:** Ground Truth, GPT-4o, InternVL3-8B, Qwen2.5-VL-7B, and Ours (ChartSpec). While base models (columns 3-4) struggle with complex layouts like Radar and Boxplots, our method (Column 5) achieves high fidelity comparable to GPT-4o. Notably, in the Boxplot (Row 3), our model successfully preserves statistical outliers (small circles) which are missed by other baselines, demonstrating the precision of our spec-based reward.

imitation to Semantically Structured Grounding, our approach leverages **Chart Specification** to drive both high-quality data curation and the **Spec-Align Reward**, effectively enforcing rigorous plotting constraints and mitigating hallucinations. Extensive experiments demonstrate that our method achieves state-of-the-art results with exceptional data efficiency, surpassing competitive baselines using only 3K samples. Future work will explore the extension of this structural paradigm to interactive chart editing via iterative self-correction mechanisms.

References

- [1] N. Siegel, S. Styles, S. K. Divvala, Figureseer: Parsing result-figures in research papers, ACM Transactions on Graphics (TOG) 35 (2016) 111.
- [2] J. Poco, J. Heer, Reverse-engineering visualizations: Recovering visual encodings from chart images, in: Proceedings of the 2017 CHI Conference on Human Factors in Computing Systems, ACM, 2017, pp. 5707–5717.
- [3] K. Kafle, B. Price, S. Cohen, C. Kanan, Dvqa: Understanding data visualizations via question answering, in: Proceedings of the IEEE Conference on Computer Vision and Pattern Recognition (CVPR), 2018, pp. 5648–5656.
- [4] J. Zhang, J. Huang, S. Jin, S. Lu, Vision-language models for vision tasks: A survey, IEEE transactions on pattern analysis and machine intelligence 46 (2024) 5625–5644.
- [5] C. Yang, C. Shi, Y. Liu, B. Shui, J. Wang, M. Jing, L. Xu, X. Zhu, S. Li, Y. Zhang, et al., Chartmimic: Evaluating lmm’s cross-modal reasoning capability via chart-to-code generation, arXiv preprint arXiv:2406.09961 (2024).
- [6] C. Wu, Y. Ge, Q. Guo, J. Wang, Z. Liang, Z. Lu, Y. Shan, P. Luo, Plot2code: A comprehensive benchmark for evaluating multi-modal large language models in code generation from scientific plots, arXiv preprint arXiv:2405.07990 (2024).
- [7] X. Zhao, X. Luo, Q. Shi, C. Chen, S. Wang, Z. Liu, M. Sun, Chartcoder: Advancing multimodal large language model for chart-to-code generation, arXiv preprint arXiv:2501.06598 (2025).
- [8] H. Lightman, et al., Let’s verify step by step, ICLR (2024).

[9] H. Le, Y. Wang, A. D. Gotmare, S. Silvio, S. C. H. Hoi, Coderl: Mastering code generation through pretrained models and deep reinforcement learning, in: NeurIPS, 2022.

[10] T. Beltramelli, pix2code: Generating code from a graphical user interface screenshot, arXiv preprint arXiv:1705.07962 (2017).

[11] Z. Zhang, Y. Cao, L. Liao, Enhancing chart-to-code generation in multimodal large language models via iterative dual preference learning, in: arXiv preprint arXiv:2504.02906, 2025.

[12] F. Liu, J. M. Eisenschlos, F. Piccinno, S. Krichene, C. Pang, K. Lee, M. Joshi, W. Chen, N. Collier, Y. Altun, DePlot: One-shot visual language reasoning by plot-to-table translation, in: A. Rogers, J. Boyd-Graber, N. Okazaki (Eds.), Findings of the Association for Computational Linguistics: ACL 2023, Association for Computational Linguistics, Toronto, Canada, 2023, pp. 10381–10399. URL: <https://aclanthology.org/2023.findings-acl.660/>. doi:10.18653/v1/2023.findings-acl.660.

[13] R. Xia, B. Zhang, H. Ye, X. Yan, Q. Liu, H. Zhou, Z. Chen, P. Ye, M. Dou, B. Shi, et al., Chartx & chartvlm: A versatile benchmark and foundation model for complicated chart reasoning, arXiv preprint arXiv:2402.12185 (2024).

[14] M. Akhtar, O. Cocarascu, E. Simperl, Reading and reasoning over chart images for evidence-based automated fact-checking, in: A. Vlachos, I. Augenstein (Eds.), Findings of the Association for Computational Linguistics: EACL 2023, Association for Computational Linguistics, Dubrovnik, Croatia, 2023, pp. 399–414. URL: <https://aclanthology.org/2023.findings-eacl.30/>. doi:10.18653/v1/2023.findings-eacl.30.

[15] Y. Wang, S. Wu, Y. Zhang, W. Wang, Z. Liu, J. Luo, H. Fei, Multimodal chain-of-thought reasoning: A comprehensive survey, arXiv preprint arXiv:2503.12605 (2025).

[16] Q. Zhao, Y. Lu, M. J. Kim, Z. Fu, Z. Zhang, Y. Wu, Z. Li, Q. Ma, S. Han, C. Finn, A. Handa, M.-Y. Liu, D. Xiang, G. Wetzstein, Cotvla: Visual chain-of-thought reasoning for vision-language-action models, in: Proceedings of the IEEE/CVF Conference on Computer Vision and Pattern Recognition (CVPR), 2025. URL: <https://arxiv.org/abs/2503.22020>.

[17] K. Lee, C. Gan, Y. Cheng, H. Li, W. Wang, X. Chen, J. Hu, L. Wang, D. Liu, Z. Chen, et al., Pix2Struct: Screenshot parsing as pretraining for visual language understanding, arXiv preprint arXiv:2210.03347 (2022). Accepted at ICML.

[18] F. Liu, F. Piccinno, S. Krichene, C. Pang, K. Lee, M. Joshi, Y. Altun, N. Collier, J. M. Eisenschlos, Matcha: Enhancing visual language pretraining with math reasoning and chart derendering, arXiv preprint arXiv:2212.09662 (2022).

[19] Z. Li, J. Fu, L. Song, J. Bian, J. Zhang, R. Wang, Chain of functions: A programmatic pipeline for fine-grained chart reasoning data, arXiv preprint arXiv:2503.16260 (2025).

[20] L. Ouyang, et al., Training language models to follow instructions with human feedback, in: NeurIPS, 2022.

[21] R. Rafailov, et al., Direct preference optimization: Your language model is secretly a reward model, in: Advances in Neural Information Processing Systems, 2023.

[22] X. Liang, J. Hu, D. Wang, Z. Ma, L. Zhao, R. Li, B. Wan, Q. Wang, Chexpo: Preference optimization for chest x-ray vlm with counterfactual rationale, in: Proceedings of the 33rd ACM International Conference on Multimedia, 2025, pp. 2606–2615.

[23] N. Lambert, J. Morrison, V. Pyatkin, S. Huang, H. Iivison, F. Brahman, L. J. V. Miranda, A. Liu, N. Dziri, S. Lyu, Y. Gu, S. Malik, V. Graf, J. D. Hwang, J. Yang, R. Le Bras, O. Tafjord, C. Wilhelm, L. Soldaini, N. A. Smith, Y. Wang, P. Dasigi, H. Hajishirzi, TÜLU 3: Pushing frontiers in open language model post-training, in: Proceedings of the Conference on Language Modeling (COLM), 2025. URL: <https://openreview.net/forum?id=i1uGbfHHpH>, arXiv:2411.15124.

[24] Z. Shao, P. Wang, Q. Zhu, R. Xu, J. Song, X. Bi, H. Zhang, M. Zhang, Y. Li, Y. Wu, et al., Deepseekmath: Pushing the limits of mathematical reasoning in open language models, arXiv preprint arXiv:2402.03300 (2024).

[25] DeepSeek-AI, Deepseek-r1: Incentivizing reasoning capability in llms via reinforcement learning, 2025. URL: <https://arxiv.org/abs/2501.12948>. arXiv:2501.12948.

[26] M. He, Y. Liu, S. Tao, Y. Luo, H. Zeng, C. Su, L. Zhang, H. Ma, D. Wei, W. Meng, et al., R1-t1: Fully incentivizing translation capability in llms via reasoning learning, arXiv preprint arXiv:2502.19735 (2025).

[27] Y. Liu, Z. Chen, S. Xu, M. He, S. Tao, W. Meng, Y. Xie, T. Han, C. Zhao, J. Du, D. Wei, S. Zhang, Y. Sun, R-log: Incentivizing log analysis capability in llms via reasoning-based reinforcement learning, 2025. URL: <https://arxiv.org/abs/2509.25987>. arXiv:2509.25987.

[28] Q. Yu, Z. Zhang, R. Zhu, et al., Dapo: An open-source llm reinforcement learning system at scale, arXiv preprint arXiv:2503.14476 (2025).

[29] C. Zheng, S. Liu, M. Li, X.-H. Chen, et al., Group sequence policy optimization, arXiv preprint arXiv:2507.18071 (2025).

[30] S. Yang, C. Dou, P. Guo, K. Lu, Q. Ju, F. Deng, R. Xin, Depo: Dynamic clipping policy optimization, arXiv preprint arXiv:2509.02333 (2025).

[31] L. Wilkinson, The grammar of graphics, in: Handbook of computational statistics: Concepts and methods, Springer, 2011, pp. 375–414.

[32] A. Satyanarayan, D. Moritz, K. Wongsuphasawat, J. Heer, Vega-lite: A grammar of interactive graphics, IEEE Transactions on Visualization and Computer Graphics 23 (2017) 341–350.

[33] Y. Han, C. Zhang, X. Chen, X. Yang, Z. Wang, G. Yu, B. Fu, H. Zhang, Chartllama: A multimodal llm for chart understanding and generation, in: Unpublished or workshop, 2023. Preprint available on HuggingFace / GitHub.

[34] J. Bai, S. Bai, S. Yang, S. Wang, S. Tan, P. Wang, J. Lin, C. Zhou, J. Zhou, Qwen2-vl: A versatile vision-language model for understanding, localization, text reading, and beyond, CoRR abs/2409.12191 (2024).

[35] S. Bai, K. Chen, X. Liu, J. Wang, W. Ge, S. Song, K. Dang, P. Wang, S. Wang, J. Tang, et al., Qwen2. 5-vl technical report, arXiv preprint arXiv:2502.13923 (2025).

[36] G. Team, Google, Gemini: a family of highly capable multimodal models, arXiv preprint arXiv:2312.11805 (2023).

[37] Anthropic, The claude 3 model family: Opus, sonnet, haiku, Anthropic Technical Report (2024).

[38] OpenAI, Gpt-4v(ision) system card, OpenAI Technical Report (2023).

[39] A. Hurst, A. Lerer, A. P. Goucher, A. Perelman, A. Ramesh, A. Clark, A. Ostrow, A. Welihinda, A. Hayes, A. Radford, et al., Gpt-4o system card, arXiv preprint arXiv:2410.21276 (2024).

[40] P. Zhang, X. Dong, Y. Zang, Y. Cao, R. Qian, L. Chen, Q. Guo, H. Duan, B. Wang, L. Ouyang, S. Zhang, W. Zhang, Y. Li, Y. Gao, P. Sun, X. Zhang, W. Li, J. Li, W. Wang, H. Yan, C. He, X. Zhang, K. Chen, J. Dai, Y. Qiao, D. Lin, J. Wang, Internlm-xcomposer-2.5: A versatile vision-language model supporting long-context input and output, CoRR abs/2407.03320 (2024).

[41] H. Lu, W. Liu, B. Zhang, B. Wang, K. Dong, B. Liu, J. Sun, T. Ren, Z. Li, Y. Sun, et al., Deepseek-vl: Towards real-world vision-language understanding, arXiv preprint arXiv:2403.05525 (2024).

[42] H. Liu, C. Li, Y. Li, B. Li, Y. Zhang, S. Shen, Y. J. Lee, Llava-next: Improved reasoning, ocr, and world knowledge, 2024. URL: <https://llava-vl.github.io/blog/2024-01-30-llava-next/>.

[43] Y. et al., Minicpm-llama3-v2.5: A gpt-4v-level multimodal llm with strong ocr and high-resolution capabilities, CoRR abs/2408.01800 (2024).

[44] F. Meng, W. Wang, Z. Zhou, H. Chen, Chartassistant: A universal chart multimodal language model via chart-to-table pre-training, arXiv preprint arXiv:2401.02384 (2024).

[45] L. Zhang, A. Hu, H. Xu, M. Yan, Y. Xu, Q. Jin, J. Zhang, F. Huang, Tinychart: Efficient chart understanding with program-of-thoughts learning and visual token merging, in: Proceedings of the 2024 Conference on Empirical Methods in Natural Language Processing (EMNLP), 2024, pp. 1882–1898. doi:10.18653/v1/2024.emnlp-main.

112.

[46] R. Xia, B. Zhang, H. Ye, X. Yan, Q. Liu, H. Zhou, Z. Chen, M. Dou, B. Shi, J. Yan, Y. Qiao, Chartx & chartvlm: A versatile benchmark and foundation model for complicated chart reasoning, arXiv preprint arXiv:2402.12185 (2024).



Minggui He received the B.E. degree from Beijing University of Chemical Technology, China and M.E. from Waseda University, Japan in 2016 and 2018 respectively. He is currently a Phd candidate in Waseda University. His research interests include Multi-modal content process and generation, large language models and image signal processing.



Mingchen Dai is currently a third-year master's student in Software Engineering at the University of Science and Technology of China. He received his B.E. degree from Qingdao University of Technology in 2021. His research interests include multi-modal large language models and chart-related analysis and generation.



Jian Zhang received the B.E. and M.E. degrees from The University of Electronic Science and Technology of China in 2016 and 2019 respectively. He was a Exchange Student with Waseda University, Japan, in 2017, and also got M.E. degree from Waseda University, Japan, in 2019. He has been a Ph.D. Student with Waseda University, Japan, since 2019. His research interests include computer vision, image processing and deep learning.



Yilun Liu received the B.S. degree from Nankai University in 2020. He received the M.S. degree in Electrical and Computer Engineering from Georgia Institute of Technology in 2022. He is currently a Research Engineer with Huawei Translation Services Center in 2012 Lab, Huawei. His research interests include log analysis, large language models, machine translation, and natural language processing.



Shimin Tao received the M.S. degree from Beijing University of Aeronautics and Astronautics, Beijing, China. He is currently a technology expert in Huawei 2012 laboratory. The main research direction is AIOps, machine translation, natural language processing, etc.



Pufan Zeng received the B.E. degree from Beijing University of Chemical Technology, China. He is currently pursuing the master's degree with the University of Science and Technology of China. His research interests include large language models and natural language processing.



Osamu Yoshie is currently a professor at Waseda University, Japan. His research interests include the analysis and synthesis of information so that a collective intelligence is generated in a community, which is composed of human, software and hardware. As an application of the community-based information processing, he is developing methodologies for consensus building in an organization, inspired from the research experience at FX Palo Alto Laboratory in USA and GMD (currently

Chart Specification

Fraunhofer) in Germany. He is a recipient of many awards from professional research societies, such as the Society of Instrument and Control Engineers (SICE), the Institute of Electrical Engineers (IEE) Japan, the Society of Plant Engineers Japan, Japan Industrial Management Association, etc. He is a fellow of IEE Japan.



Yuya Ieiri received the B.Eng., M.Eng., and Ph.D. degrees in Engineering from Waseda University, Japan, in 2017, 2019, and 2021, respectively. He is currently an Assistant Professor at Waseda University. His research interests include artificial intelligence, human-computer interaction, social systems engineering, augmented reality, tourism informatics, and social informatics.